Available online at www.sciencedirect.com
SCIENCE DIRECT®
International Journal of Solids and Structures 42 (2005) 1883–1907
INTERNATIONAL JOURNAL OF SOLIDS and STRUCTURES
www.elsevier.com/locate/ijsolstr

Numerical modelling of nonlinear response of soil. Part 2: Strain localization investigation on sand

X. Liu *, A. Scarpas, J. Blaauwendraad

Faculty of Civil Engineering and Geosciences, Section of Structural Mechanics, Delft University of Technology, Stevinweg 1, 2628CN Delft, The Netherlands

Received 14 September 2004
Available online 27 October 2004

Abstract

In this contribution, numerical investigations of strain localization have been performed on 3D dense saturated sand specimens subjected to triaxial loading conditions. The importance of the presence of fluid on the formation and evolution of strain localization are identified by several analyses. The role of the fluid components on strain localization is addressed computationally. The important influencing factors, such as soil permeability; water suction; draining conditions and specimen geometry on strain localization development and the formation of localization pattern are presented in detail. Mesh sensitivity issues have been studied by means of both, a one-dimensional wet soil bar subjected to dynamic compression load and, a 3D saturated specimen subjected to triaxial loads. It has been shown that, in a multiphase material, the fluid (water) phase plays indeed an important role in strain localization. The formation and evolution of strain localization are influenced both by the material behaviour of the media and the interaction between fluid and solid components. A companion paper focuses on the development of the constitutive model to simulate the soil response in the elastoplastic range has been addressed, and a general procedure has been developed for determination of the material parameters of the constitutive model.

Keywords: Strain localization; Interaction; Soil permeability; Suction; Cavitations; Fluid and solid; Excess pore water pressure

1. Introduction

The analysis of strain localization is of importance in engineering practice because localization is a precursor to sudden failure. Localized deformations in the form of narrow shear bands are often observed to

* Corresponding author. Tel.: +31 15 2787918; fax: +31 15 2785767.
E-mail address: x.liu@citg.tudelft.nl (X. Liu).

0020-7683/$ - see front matter © 2004 Elsevier Ltd. All rights reserved.
doi:10.1016/j.ijsolstr.2004.09.008

develop after large inelastic deformation in materials. Within this shear band, the material behaviour is inelastic. The width and orientation of these shear bands depend on material parameters, geometry, boundary conditions and loading conditions. In other words, knowledge concerning the development of the strain localization phenomenon will also lead to insight into failure mechanisms.

Typical examples of material that prone to strain localization are frictional materials such as concrete, rocks and soils. These materials show a reduction of load carrying capacity, after reaching the limit load, accompanied by increasing localized deformations. The mechanism responsible for strain localization can vary widely from one material to another. Normally strain localization is treated as the result of local inhomogeneities, stress concentrations or the onset of some physical mechanism that degrades abruptly the strength of the material at one point. Alternatively, strain localization can be considered as a bifurcation from a smoothly varying pattern of deformation, which arises as a result of instability in the inelastic behaviour of the material.

Strain localization has been extensively studied in recent years, in particular in connection with single phase solids. Among others Needleman (1988), Loret and Prevost (1990) and Sluys (1992), have investigated the problem of dynamic strain localization in single phase solids. It is demonstrated that generalizations and modifications of standard continuum plasticity can overcome some of the numerical problems associated with localization, like severe mesh dependence and non-convergence.

Since the end of the 70s, several authors have studied strain localization in multiphase materials. Rudnicki (1984) analyzed a fluid saturated rock mass with an embedded weakened layer. Rice (1985) studied the effect of material dilatancy on strain localization in fully saturated fractional material. Vardoulakis (1986) showed the importance of dynamic stability analysis in case of undrained simple-shear deformation of water-saturated granular soil. Loret and Prevost (1991) studied the formation of localization in a fully saturated soil specimen using dynamic strain localization theory. A model based on the general framework of averaging theories and capable of simulating shear band dominated processes in saturated porous media was presented by Schrefler et al. (1995, 1996).

In recent years, much effort has been devoted to devise regularization strategies to simulate the development of shear band in multiphase materials without mesh dependency. According to studies, e.g. Schrefler et al. (1995), Schrefler et al. (1996), Liu et al. (2001) and Liu (2003), numerical simulation of strain localization in a multiphase material have evidenced that mesh dependency is not severe as in single phase materials. The reason is that in the governing field equations a gradient term is included through Darcy's law, an internal length scale is introduced naturally, resulting thus to a regularization for strain localization (Loret and Prevost, 1991 and Schrefler et al., 1995). This internal length scale depends on several material parameters and in particular on the permeability. Reliable experimental observations have been difficult to make and the physical understanding of the nature of the problem is not yet satisfactory.

In order to properly characterize the mechanisms of strain localization, the investigations of strain localization are needed both numerically and experimentally. In recent years, several researchers have carried out extensively numerical and experimental investigations of strain localization in biaxial tests, e.g. Vardoulakis (1980), Tatsuoka et al. (1990), Desrues et al. (1985), Han and Vardoulakis (1991), Mokni and Desrues (1998), Karstunen (1999) and others. Biaxial tests have proven to be suitable for the detection of strain localization. This is because biaxial apparatus allows free shear band formation and visual inspection of the sample throughout the test.

In soil mechanics, triaxial tests are widely utilized to perform soil mechanical identifications. However, due to the characteristics of the setup, to use these tests for the detection of strain localization is more difficult. Therefore, the mechanisms of strain localization in these tests have been investigated less thoroughly. Lade (1982) experimentally investigated the localization effects in triaxial tests on dense sand. The test results showed the difficulty in detecting strain localization in the test condition. Desrues et al. (1996) used computer tomography to study strain localization in sand specimens subjected to axisymmetric triaxial loading. The inception and the development of localization were detected and described.

Up to now, very few numerical studies on strain localization in triaxial tests have been done, especially for multiphase materials. To the best of the author's knowledge, only Leroy and Ortiz (1990) illustrated the effect of geometry and boundary conditions on strain localization in a specimen subjected to axisymmetric triaxial loads. Harireche and Loret (1992) applied the visco-plasticity regularization procedure to study shear band pattern transition in true triaxial compression tests.

From all the above studies it can be concluded that, due to the complexities associated with solid fluid phase interactions, the mechanisms responsible for strain localization in multiphase material media can vary significantly from case to case. Several problems need to be addressed such as: the role of the fluid components in localization, the significant influencing factors in the development of strain localization, the question of why localization pattern vary between different tests, how the constitutive model can be regularized to avoid mesh sensitivity (as it frequently occurs in single phase material simulations).

The aim of this investigation is to provide insight into the phenomenon of strain localization in fluid saturated sands by means of finite element analyses. In order to achieve this goal, a fully saturated 3D sand specimen subjected to true triaxial loads is chosen for numerical investigation. The importance of the presence of fluid on the formation and evolution of strain localization is identified. The role of influencing factors, such as soil permeability, water suction and draining conditions will be presented. Also, the influence of specimen geometry is illustrated. Various combinations of specimen geometry and material characteristics are examined.

In order to investigate the significance of the regularizing influence of the presence of the fluid on shear band formation and mesh independency, analyses are carried out in the last part of this contribution on strain localization in a one-dimensional soil bar subjected to dynamic compression load and on a three-dimensional specimen subjected to triaxial loading. The influence of the permeability on the width of the shear band is investigated numerically. It is shown that due to the presence of an internal length scale within, mesh independence can be ensured.

2. Strain localization in 3D specimen

2.1. Specimen geometry and material characteristics

A fully saturated cubic 3D specimen with impermeable boundaries is selected for the numerical simulations. The finite element mesh consists of 20-nodded brick elements, Fig. 1. The height and width of the specimen are constant but the thickness is varied in the z direction. The geometry parameters of the specimen are given in Table 1. Because of symmetry, only half of the specimen thickness is simulated.

A confining pressure of 150 kPa is applied to all boundaries of the specimen and kept constant throughout the analysis. Incremental displacements are applied on a rigid platen at the top of the specimen. The left, right and front planes of the specimen can move freely in the normal direction of each plane. The bottom plane of the specimen is constrained in the y-direction. In order to simulate the real test conditions, interface elements are introduced at the top and the bottom of the sand specimen between the rigid platens and the specimen. By adjusting the bond stiffness D_{tt} of the interfaces, the influence of the roughness of the platen on strain localization within the specimen can be simulated.

According to experiment observations (e.g. Arthur et al., 1977; Vardoulakis, 1980; Desrues et al., 1985; Han and Vardoulakis, 1991; Mokni and Desrues, 1998), distinct shear bands often occur in dense sand specimens under both drained and undrained conditions. Therefore, in this study, dense sand is chosen for the numerical investigation. The material parameters have been derived on the basis of triaxial tests on 'Eastern Scheldt' dense sand and are shown in Table 1. The nonassociative constitutive model described in the companion paper under the assumption of small deformations is chosen to simulate the material nonlinear response.

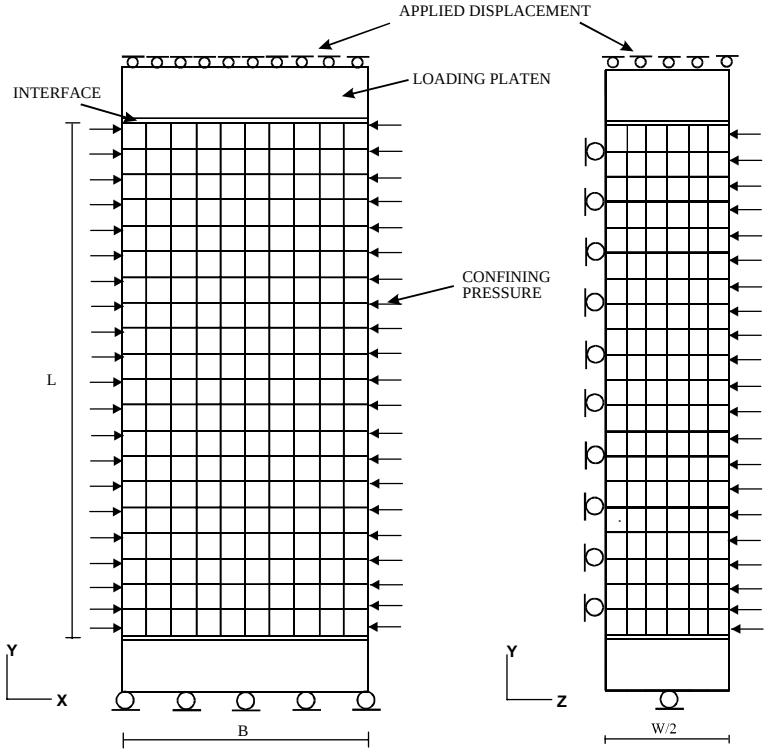

Fig. 1. Schematic of 3D specimen geometry and loading conditions.

Table 1
Main material parameters and specimen geometry data

E (MPa)	79	g	1.795	k_w (m/s)	1.0e−04–1.0e−10
v	0.29	a_1	1.17e−03	ρ_s (kg/m^3)	2.0e−03
λ	0.0055	b_1	−3044	D_{tt} (MPa)	0.001–0.01
κ	0.0025	d_1	5.53e−03	L (mm)	100
n	5.04	κ_c	0.47	B (mm)	50
γ	0.155	κ_1	3.5	W (mm)	10–80

2.1.1. Evolution of strain localization

The specimen in Fig. 1 consisting of 800 elements, with height $L = 100$ mm, width $B = 50$ mm and thickness $W = 10$ mm is investigated first. Initially, the deformation of the specimen is nearly homogenous. After a vertical displacement of 0.485 mm, a symmetric shear band initiated from the corners of the top and bottom surfaces of the specimen, near the platens, and gradually propagated along the diagonal direction of specimen, Fig. 2(a) and (b). As the vertical displacement increases to 1.185 mm, the specimen is bulging out more and four regions of high effective plastic strain appear symmetrically around the center of the specimen, see Fig. 2(c). Finally, two pairs of dominant shear bands emanated from these defects and propagated towards the boundaries of the specimen, Fig. 2(d).

The effective plastic strains at different vertical displacement levels along a vertical cross-section at $x = 11.3$ mm are plotted in Fig. 3. It can be observed that the development of the plastic deformations in the specimen starts from a homogenous state and gradually changes to an extremely inhomogeneous

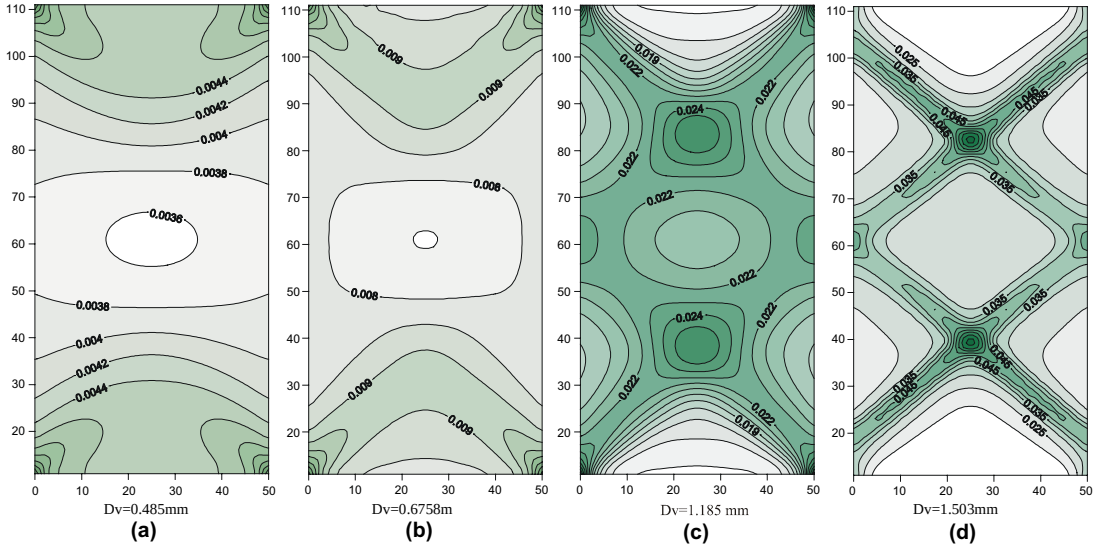

Fig. 2. Contours of effective plastic strain at different vertical displacements (D_v) in a specimen with $k_w = 1.0e{-}06\,m/s$.

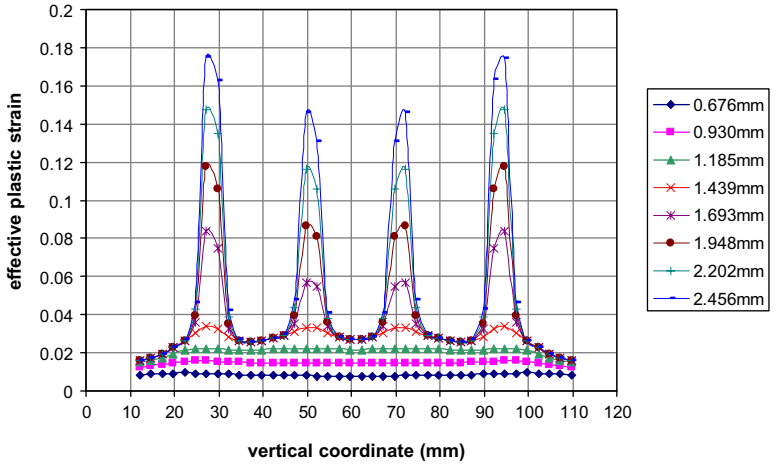

Fig. 3. Development of effective plastic strains along a cross section at $x = 11.3\,mm$ for different vertical displacements (D_v).

one. The distribution of the effective plastic strain is maintained symmetrically along the cross-section of the specimen. The higher intensity of the effective plastic strain occurs in the bands near the loading platens. The actual deformed mesh at a vertical displacement of 1.503 mm is shown in Fig. 4.

2.1.2. *Effects of soil permeability*

In order to investigate the influence of soil permeability on the conditions leading to the development of strain localization, the response of specimens with permeability $k_w = 1.0e{-}04\,m/s$, $k_w = 1.0e{-}06\,m/s$ and $k_w = 1.0e{-}10\,m/s$ are examined respectively. The response of these specimens, at the same level of vertical displacement, is compared in Fig. 5. The corresponding contours of excess pore water pressure are presented in Fig. 6 (in the code, positive pore water pressure corresponds to suction).

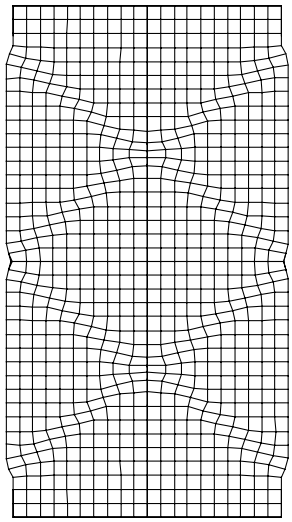

Fig. 4. Actual deformed mesh at $D_v = 1.503$ mm.

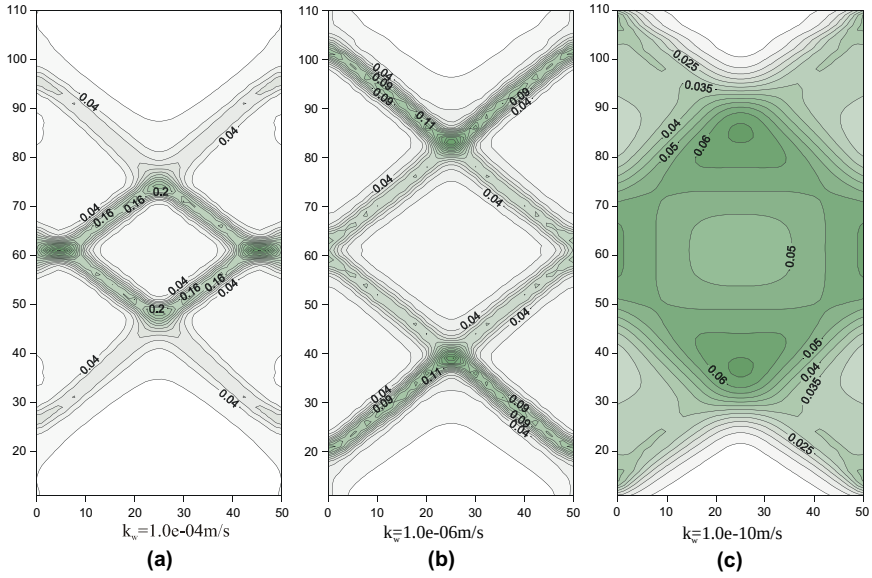

Fig. 5. Contours of effective plastic strain at same vertical displacement.

As expected, for the lower permeability specimen, higher water suction is generated. This higher water suction results to increase in the shear strength of the sand and thus to reduced levels of plastic deformation in the shear bands. The higher the water suction, the later localization will occur. It can be observed also that the shear band thickness is influenced significantly by the soil permeability, the higher the permeability the thinner the shear bands.

Not only shear band thickness but also the development of the shear band in the specimen is influenced by soil permeability. For the case with higher permeability, the shear bands are initiated and developed

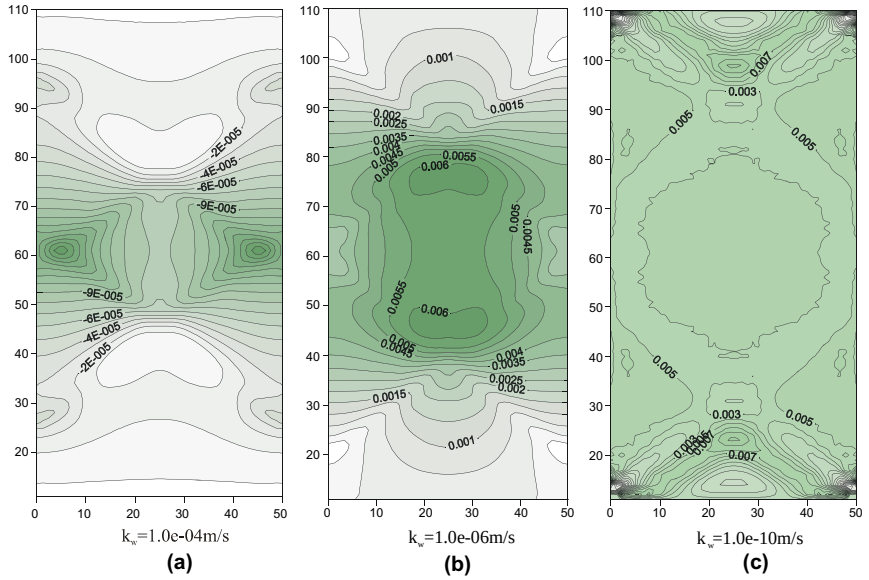

Fig. 6. Contours of excess pore water pressure at same vertical displacement.

around the center of the specimen. For the specimen with lower permeability, higher water suction is created and concentrated around the central part of the specimen, thus severe strain localization occurs only in the bands near the loading platens.

As can be seen from the load-deformation curves in Fig. 7, for the specimen with higher permeability, strain localization occurs at a vertical displacement level lower than the specimen with lower permeability. This observation coincides with the experimental results.

It can be concluded that the permeability affects the degree of coupling between the solid and the fluid phases and that it plays an important role in the development of strain localization. The lower its value, the

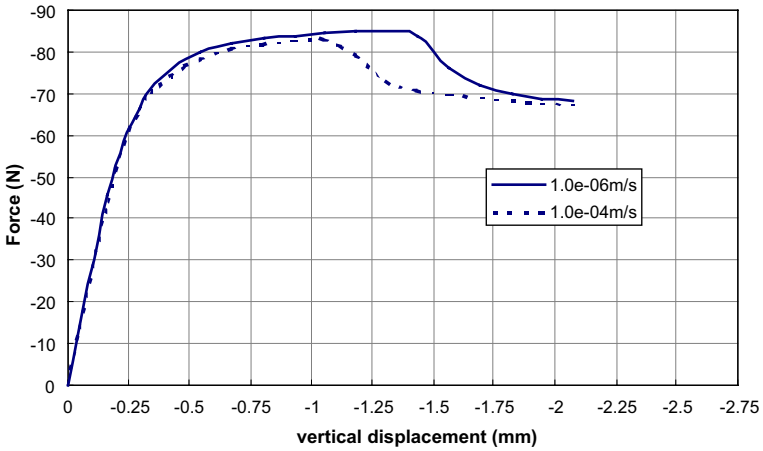

Fig. 7. Load-deformation curve for specimen with different permeability.

higher is the part of the load increment taken by water and the slower is the transfer of load to the solid skeleton. Hence coupling effects increase as the permeability decreases.

2.1.3. Effects of pore water suction

According to laboratory observations, in a drained test, depending on the stress level, granular materials exhibit a dilatant or contractive response. In an undrained test, due to the incompressibility of the fluid, the tendency to dilate or to contract will induce pore water pressure variations. As indicated in the previous section, the dilatancy of the material can build up positive excess pore water pressure (suction) in the specimen and hence increase the shear strength of the soil. It was already observed that the onset and development of strain localization are related to the water suction in the specimen, Fig. 6. In this section, the emphasis lies on the relation between water suction and the occurrence of strain localization.

The same specimen utilized in the previous section has been chosen as the numerical example. Figs. 8–10 present the plots of excess water pressure, water flow direction, as well as the corresponding effective plastic strains in the specimen. It can be observed that initially, the distribution of the water suction field in the specimen is nearly homogenous and only minor concentrations of plastic strain occur at the corners of the top and bottom surfaces of the specimen, Fig. 8. In such conditions, the undrained specimen is constrained to isochoric deformation (i.e. deformation without volume change).

At a vertical displacement of 1.5025 mm, four regions of high effective plastic strain develop symmetrically around the central part of the specimen, Fig. 9(c). These cause uneven gradients of excess pore water pressure, Fig. 9(a) and hence flow towards the center of the specimen, Fig. 9(b).

At a vertical displacement of 1.6297 mm, two pairs of dominant shear bands formed and propagated to the boundaries of the specimen, Fig. 10(c). During shear band development, large material dilatancy occurs inside the shear bands. As a consequence, high excess pore pressure gradients develop within the dilated regions, Fig 10(a), and water flows mostly towards them, Fig. 10(b).

The variations of excess pore water pressure inside and outside the shear bands are compared in Fig. 11. It is observed that, due to the contraction of sand at the beginning of loading, negative excess pore water

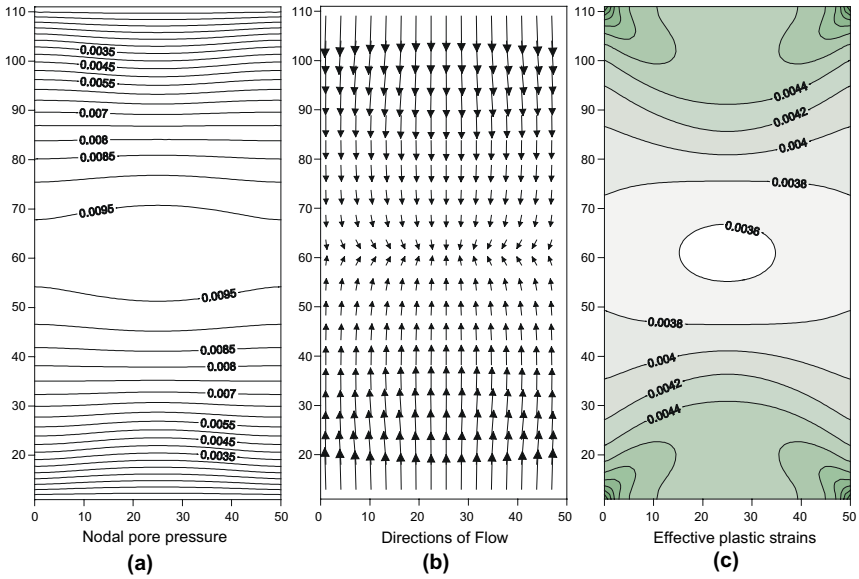

Fig. 8. Plots at vertical displacement = 0.485 mm.

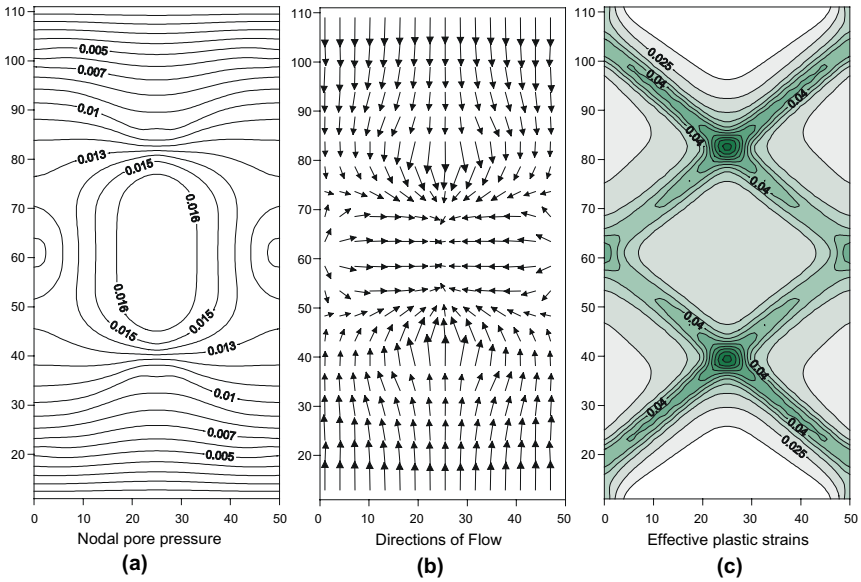

Fig. 9. Plots at vertical displacement = 1.5025 mm.

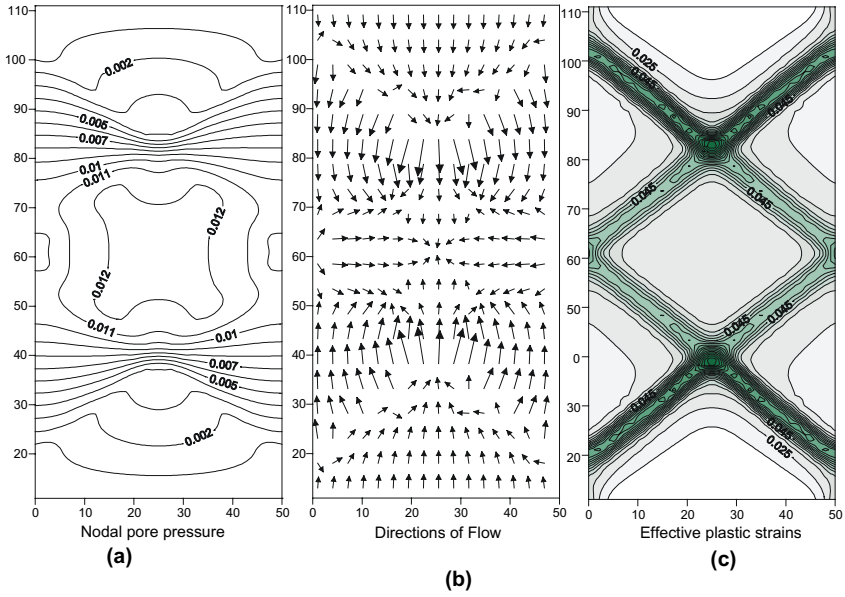

Fig. 10. Plots at vertical displacement = 1.6297 mm.

pressure (compression) is built initially. As soon as the vertical displacement of the loading platen increases to a certain value, the sand starts to dilate and hence positive excess water pressure appears. At the onset of localization, an abrupt jump of the positive excess water pressure inside the shear band can be observed. This jump of positive water pressure may relate to the fluid cavitation phenomena as indicated by Schrefler et al. (1996), Gawin et al. (1998) and Mokni and Desrues (1998).

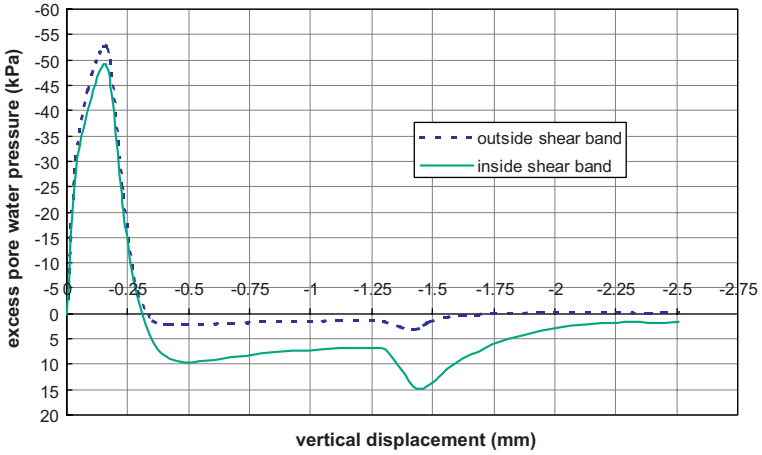

Fig. 11. Comparison of excess pore water pressure inside and outside shear band.

At cavitation, the fluid phase changes to vapour, a phenomenon that occurs when the water pressure decreases below the vapour saturation pressure. Vapour can dilate almost freely and this results to pore volume increase in the specimen. In such conditions, the undrained specimen cannot be constrained to isochoric deformation.

Fig. 12 presents the variations of excess water pressure at the intersection point of the shear bands and the corresponding load-deformation curves for three dense sand specimens (indicated by cases 1–3). It can be seen that, in all three cases, the abrupt jump of the positive excess pressure tends toward the same final value, which means that all tests start to cavitate at the same pore pressure and also that, strain localization takes place the moment when cavitation occurs.

These observations cannot be attributed to accidental phenomena, because in that case there would be no reason for the pore pressure value at localization to be the same in the three cases. The results obtained allow us to conclude that for dense sands under undrained conditions it is cavitation of the pore water that

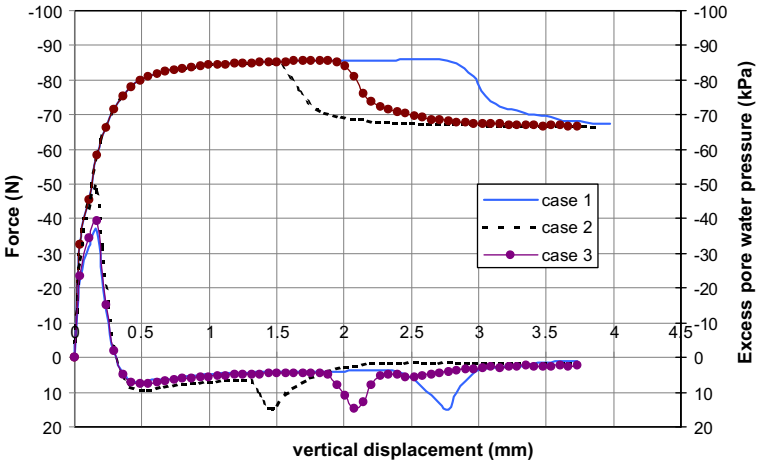

Fig. 12. Comparison of load-deformation curves and excess water pressure inside shear band for three undrained specimens.

leads to strain localization, and not vice versa. These numerical observations coincide with the experimental observations carried out on biaxial undrained tests for Hostun RF dense sand by Mokni and Desrues (1998). They stated that in these tests localization starts only after cavitation takes place.

The magnitude of confining pressure can influence water suction in the specimen. For instance, the variations of excess water pressure inside the shear band for a specimen with two confining pressures, 150 and 400 kPa, are shown in Fig. 13. It can be observed that in specimens with higher confining pressure, higher suction develops in the shear band.

As shown in Fig. 14, at the onset of localization, the magnitude of the maximum force carried by the specimen with higher confinement is much higher than the specimen with lower confinement. It can be seen that for specimens with higher confinement, strain localization occurs at vertical displacement levels much higher than in specimens with lower confinement.

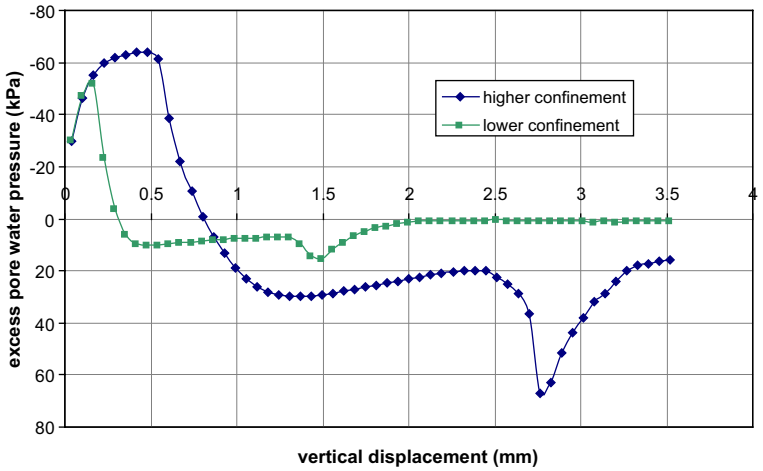

Fig. 13. Comparison of excess water pressure inside shear band for specimen with different confining pressures.

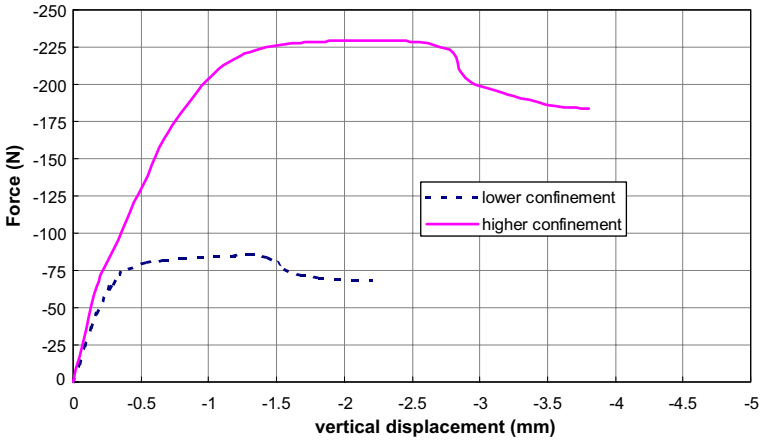

Fig. 14. Load-deformation curves for specimen with different confinement pressures.

2.1.4. Effects of draining conditions

In natural sand deposits, due to rather high permeability, material failure under static loading occurs mostly under drained conditions. Nevertheless, in some situations, undrained conditions exist. In laboratory tests, undrained conditions can be simulated by imposing impervious boundaries to the specimen to prevent water flow at the specimen boundaries. Vardoulakis (1996a,b) stated that the notion of undrained condition is meaningless on the local scale because of possible exchange of pore water between dilating and contracting in shear bands. Therefore, it is concluded by Desrues (1996) that the undrained condition is enforced only globally and is locally relaxed.

Experiments concerning strain localization in sands have been performed under both, drained and undrained conditions by several researchers, e.g. Arthur et al. (1977), Vardoulakis (1980), Desrues et al. (1985), Han and Vardoulakis (1991) and Mokni and Desrues (1998). The test results showed that, in both conditions, strain localization can occur at least on dense and medium dense sands. However, due to the influence of fluid flow, there are significant differences in the mechanical response between the two draining conditions. Those differences can influence the onset and development of strain localization in the specimen.

In order to examine the influence of draining conditions on strain localization, a specimen similar to that used in the previous section under drained and undrained conditions has been chosen as the numerical example. Fig. 15 presents the deformed meshes and the contours of effective plastic strains at the same vertical displacement level (8 mm).

It can be observed that, under drained conditions, two pairs of shear bands intersect symmetrically at the center of the specimen and that, severe damage occurs at the band intersection points. In contrast, in the specimen under undrained conditions, due to the higher water suction at the central part of the specimen, shear bands occur near the loading platens and no intersections between the two pairs of shear bands can be observed.

The thickness of the shear band is not influenced very much by the draining condition, but the intensity of the effective plastic strain in the shear bands is. The larger effective plastic strains are developed in the specimen under drained conditions. This numerical observation coincides with the experimental observations presented by Mokni (1992).

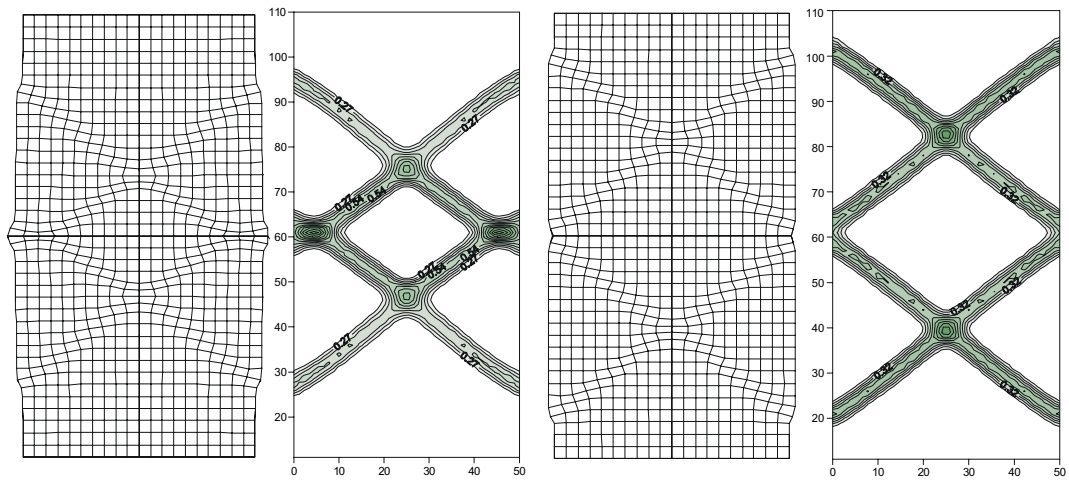

Fig. 15. Comparison of deformed mesh and effective plastic strain for specimen under different draining conditions.

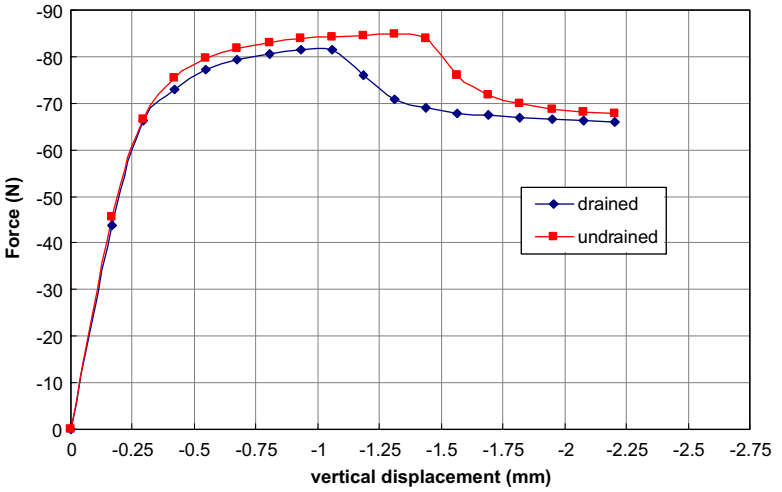

Fig. 16. Comparison of load-deformation curves for specimens under different draining conditions.

The load-deformation curves for the specimen under different draining conditions have been plotted in Fig. 16. It can be seen that, under drained conditions, strain localization occurs at a vertical displacement level lower than in the undrained case. For the specimen under undrained conditions, the actual magnitude of the maximum force at the onset of localization is higher than that in the specimen under drained condition. This can be explained by reference to Figs. 17 and 18 that show effective stress paths for the undrained and the drained specimen.

In the p'–q plane, under undrained conditions, as soon as the stress path crosses the characteristic line, dilatancy occurs in the specimen. This is accompanied by pore suction and hence an increase in the mean

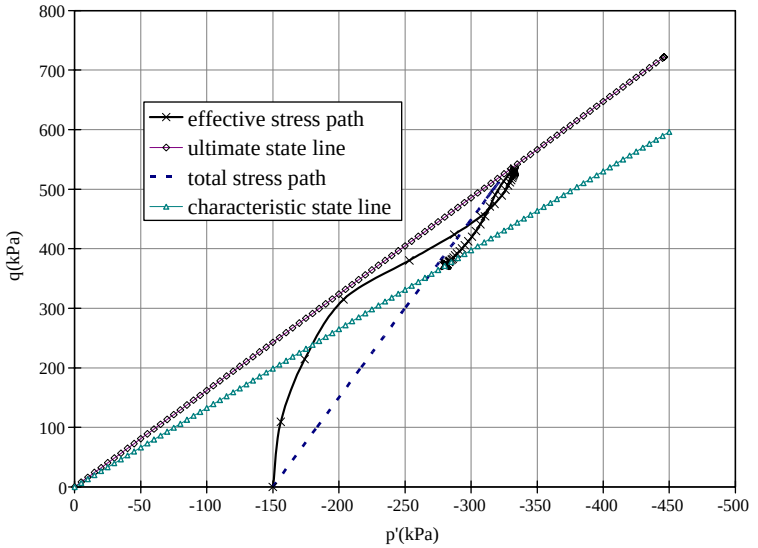

Fig. 17. Effective stress path for specimen under undrained conditions.

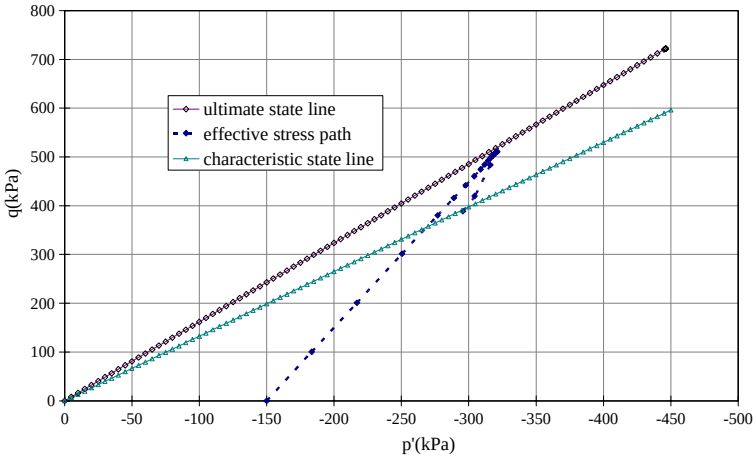

Fig. 18. Effective stress path for specimen under drained conditions.

effective stress, Fig. 17, in comparison with the drained case in which the effective stress path coincides with the stress path, Fig. 18.

2.1.5. Effects of specimen geometry

According to experimental observations, strain localization can in principle be found in all types of tests (biaxial, axisymmetric triaxial, true triaxial etc.) However, depending on test conditions, it manifests itself

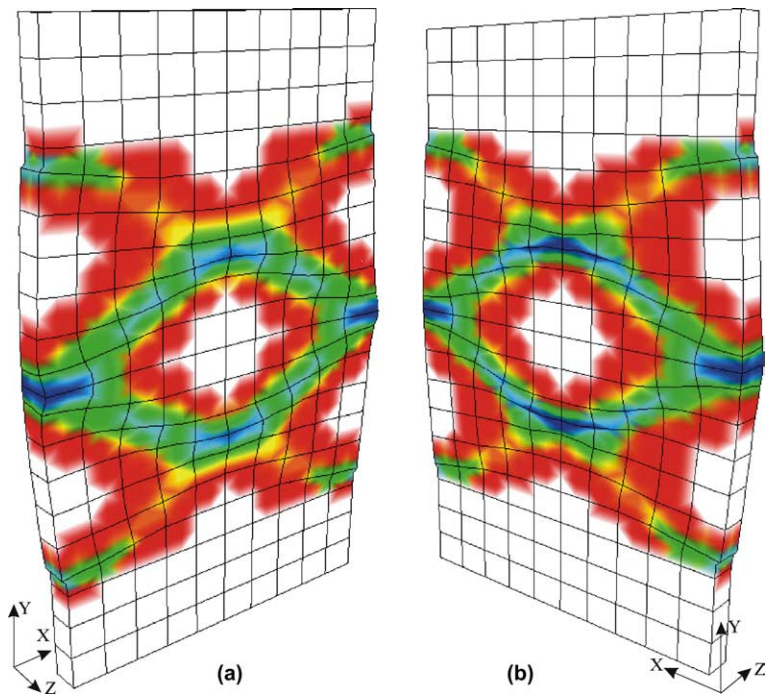

Fig. 19. Plots of shear band *pattern A* in a 3D specimen ($w = 10\,\text{mm}$) (a) front section, (b) middle section.

in different patterns. Desrues et al. (1985) observed complex localization patterns with two different sets of apparatus (true triaxial and biaxial) on dry dense sand and some combinations of shear band mechanisms in true triaxial tests. Vardoulakis (1979) and Desrues (1996) observed that specimens in an axisymmetric triaxial test deform predominantly in a barreling mode, with no evidence of localization up to very large imposed deformations. This behaviour is in sharp contrast to that of specimens in biaxial test, where localization occurs readily after the early stages of the deformation.

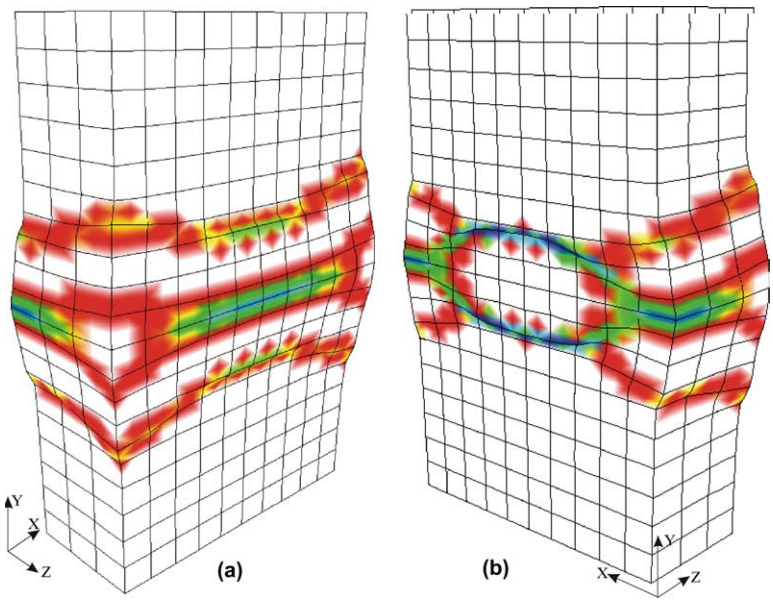

Fig. 20. Plots of shear band *pattern B* in a 3D specimen ($w = 50$ mm) (a) front section, (b) middle section.

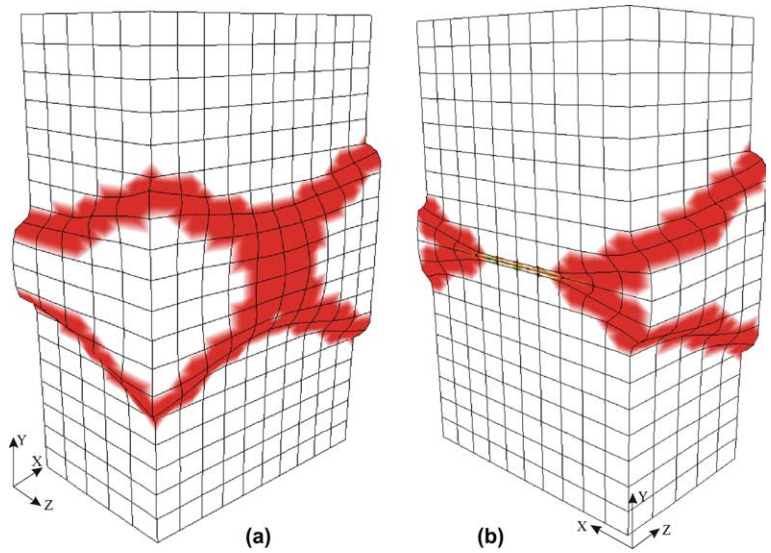

Fig. 21. Plots of shear band *pattern C* in a 3D specimen ($w = 80$ mm) (a) front section, (b) middle section.

In this investigation, similar specimens as used in the previous section are chosen to illustrate the effects of specimen geometry on strain localization. Particular attention is devoted to the transition between localization patterns. The thickness w of the specimen is varied from 10 to 80 mm in the z-direction. Because of symmetry, only half the thickness of the specimen is simulated. A constant confining pressure of 150 kPa is applied throughout the analysis.

Figs. 19–21 present the influence of the specimen thickness on the localization patterns and the transition between those patterns. In these figures, in order to clarify the formation of localization patterns, the front and middle sections of the deformed mesh together with the contours of effective plastic strain are shown. A displacement magnification factor of one is utilized in plotting these figures.

By examining first the specimen with thickness $w = 10$ mm in Fig. 19, the shear bands are initiated and evolve symmetrically at the mid-left and mid-right of the specimen sides, propagating at approximately 45° towards the mid-up and mid-down directions of the specimen. As the vertical displacement increases, two pairs of dominant shear bands are developed and emanate towards the boundaries of the specimen. It can be observed that the localization pattern in the front section of the specimen is similar as in the middle one. However, larger effective plastic strains occur in the bands at the middle section of the specimen. The distribution of the shear band in the specimen resembles a 'honeycomb-like' shape. This shear band pattern is referred to as *pattern A*.

When the specimen thickness is increased to $w = 50$ mm, two pairs of symmetric shear bands initiate and evolve at the middle section of the specimen, developing towards the sides and finally propagating to the front section of the specimen, Fig. 20. During the development of localization, the specimen is bulging out more until the deformation becomes inhomogeneous and two pairs of dominant shear bands are

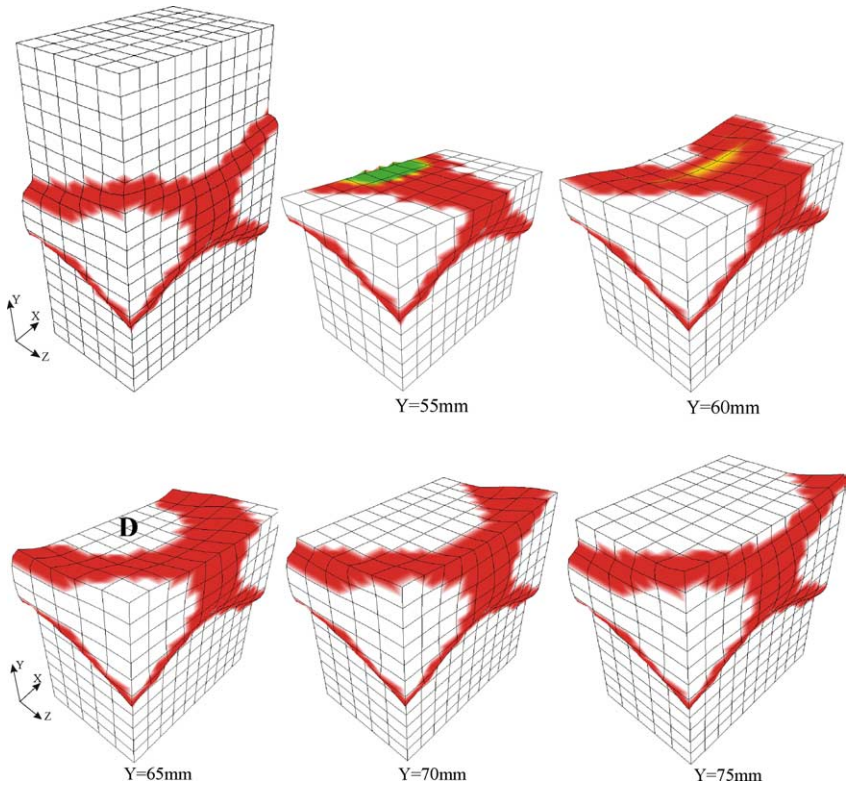

Fig. 22. Localization zones inside a 3D specimen ($W = 80$ mm) along different cross-sections.

formed and located closely in the middle of the specimen. Higher intensity effective plastic strains occur again in the bands at the middle section of the specimen. The distribution of the shear band in the specimen is in 'crab-like' shape. This shear band pattern is referred to as *pattern B*.

The results for specimen with thickness $w = 80\,\text{mm}$ are presented in Fig. 21. The shear band pattern is completely different from the previous simulations. Only one shear band initiates at the middle section of the specimen and evolves to the front section. After significant bulging, wedge systems are formed and the middle parts of the specimen between the bands move horizontally towards the specimen boundaries while the main top and bottom wedges continue moving vertically. The higher intensity of the effective plastic strain occurs again in the bands at the middle section of the specimen. The distribution of the shear band in the specimen has a 'pyramid-like' shape. This shear band pattern is referred to as *pattern C*.

In order to clarify the distribution of shear bands inside the specimen with thickness $w = 80\,\text{mm}$, several cross sections along the y-axis are shown in Fig. 22. It can be observed that, due to bulging of the specimen, cones (at location indicated as D in Fig. 22) develop inside the specimen. The cones are delimited by the adjacent shear bands where large sliding displacements occur. The material within the cone is not significantly damaged. In contrast to biaxial testing results, the localization zones are not perfectly planar and separate the half specimen into four pieces of individual slipping blocks. Higher effective plastic strains occur at the center of the specimen.

In conclusion, it can be stated that, the thickness of the 3D specimen influences significantly the distribution of shear bands within the specimen. Bulging of the specimen becomes significant when the thickness is increased. Localization divides the specimen into well-defined blocks that, at the final stages of specimen response, move with respect to each other like rigid bodies. According to the numerical observations, it is interesting to note that the transition among the shear band patterns from A to C is smooth and always associated with the specimen thickness variation.

3. Mesh sensitivity analysis

Numerical simulations of strain localization by means of the finite element method are known to lead to mesh sensitivity when the classical continuum models without enrichment are considered. Needleman (1988), Loret and Prevost (1990) Sluys (1992), and others have demonstrated that, the use of classical rate-independent continuum models for strain localization simulation can result in ill-posed problems in the numerical solution of the governing field equations. For example, loss of hyperbolicity of the equations in dynamic initial value problem. The numerical manifestation of this pathological behaviour is the localization of deformations in the finite element mesh in zones where the thickness tends to zero as the element mesh is refined. This is against experimental evidence.

In order to obtain a meaningful representation of the continuum response in the presence of strain localization, much effort has been devoted in recent years to devise regularization strategies which are able to both, simulate the development of shear band independent of the finite element mesh and, retain the nature of the governing equations. In the case of single phase solids, extended continuum formulations with internal length scales are widely used, such as the rate dependent constitutive model presented by Needleman (1988), Loret and Prevost (1990) and Sluys (1992), micropolar continua (Mühlhaus and Vardoulakis, 1987), viscoplastic models as studied by Sluys and de Borst (1992), non-local integral models by Eringen and Edelen (1972) and gradient dependent models by Mühlhaus and Aifantis (1991).

Rate or gradient dependency of the constitutive model has been shown to naturally introduce an internal length-scale parameter into the solution of the initial value problem that can prevent loss of hyperbolicity in dynamic equations or loss of ellipticity in static equations. Mesh independence can then be ensured.

In porous media strain localization, because of the presence of the gradient term in the fluid continuity equation through Darcy's law, an internal length scale is introduced naturally (Liu, 2003). This internal

length scale depends on several material parameters and in particular on the permeability. For the case of one-dimensional, fully or partially saturated, porous medium under dynamic loading, an internal length scale has been derived by Zhang et al. (1999) and later extended to the three-dimensional case (Zhang and Schrefler, 2001).

In this section, in order to investigate the significance of this regularization, numerical analyses have been carried out both on a one-dimensional soil bar subjected to dynamic compression load and a three-dimensional specimen subjected to triaxial loads. The findings of Zhang et al. (1999) are combined with the proposed nonassociative constitutive model and applied to the numerical investigation of the dynamic response of the porous media. The influence of permeability on the width of the shear band through the internal length scale is investigated numerically.

Example 1: One dimensional bar in compression

In the first example, the mesh sensitivity issue is demonstrated by means of a one-dimensional saturated soil bar compression test, Fig. 23. The bar is fixed on the left end and loaded by a dynamic constant compression force at the right end. The right end is free to drain while all other specimen boundaries are impermeable. The length L of the bar is 100 mm and the cross section area is 1 mm^2. According to the wave propagation theory, when the compression wave reaches the left fixed end of the bar, an increase of stresses due to wave reflection occurs. Therefore, in this simulation, 70% of the material compressive strength value is chosen as the magnitude of the applied load. The 'Eastern Scheldt' sand is chosen as the simulation material. The model parameters are shown in Table 1. Several permeability values are specified. In order to ver-

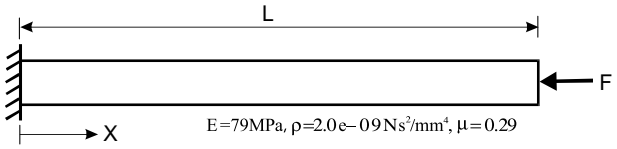

Fig. 23. One dimensional bar in compression (saturated).

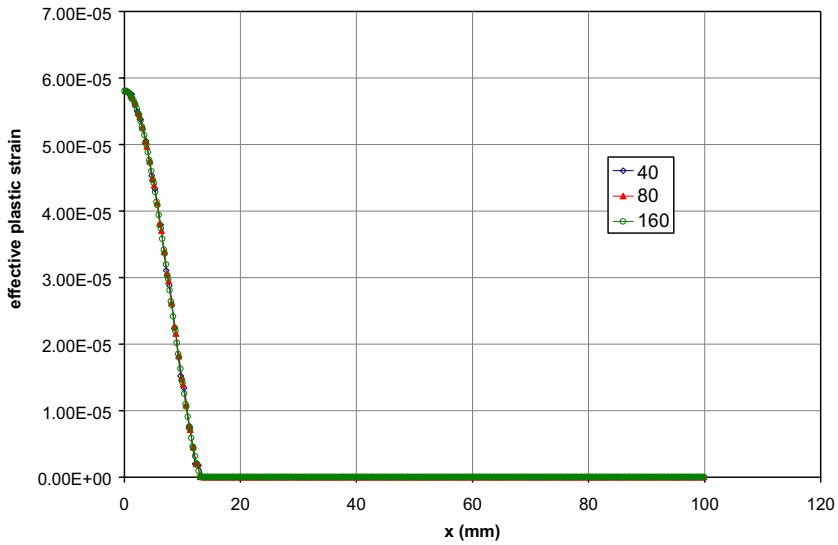

Fig. 24. Effective plastic strain distribution along saturated bar with permeability 6.e−02 m/s.

ify the mesh insensitivity of the model, the finite element meshes consisting of 40, 80, 160 elements are examined respectively.

In Fig. 24 comparisons of the effective plastic strain distribution along the saturated bar simulated with different number of elements are plotted at time 5.74e−04 s. At this moment, the compressive waves have reached the left boundary of the bar and wave reflection has been initiated. It is obvious that the three meshes give almost identical results. The localization zone in the bar converges to a finite bandwidth without dependency on mesh refinement. Apparently, the length scale parameter naturally introduced by the

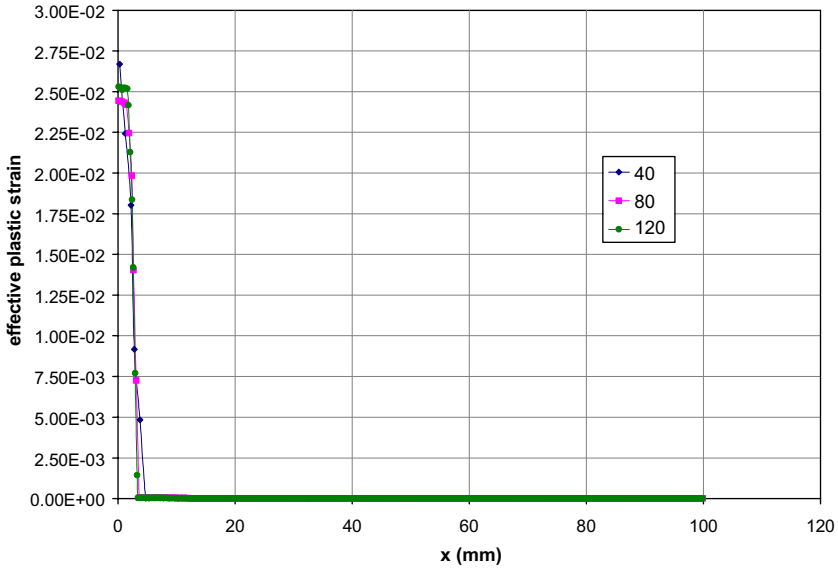

Fig. 25. Effective plastic strain distribution along dry bar.

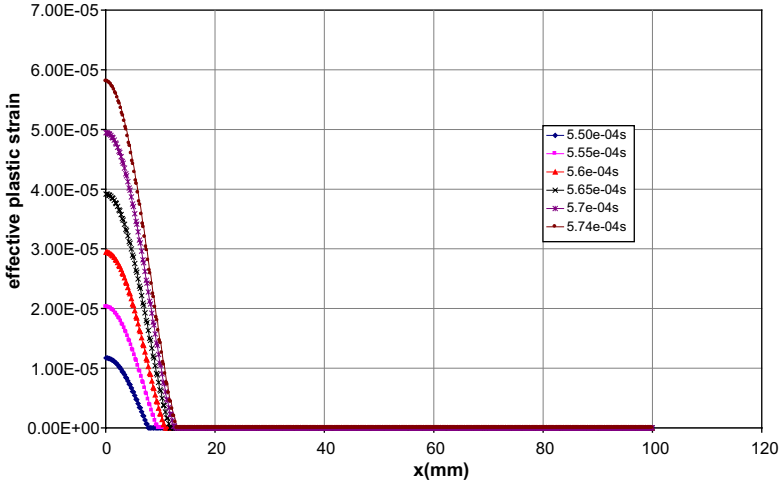

Fig. 26. In time development of effective plastic strain in saturated bar with permeability 6.e−02 m/s.

gradient term in the fluid continuity equation can indeed prevent loss of hyperbolicity during material softening and hence mesh independence is obtained.

In case of a dry bar, that is, without the beneficial effect of fluid regularization, mesh dependency appears, Fig. 25. Also, as the number of elements increases, progressively thinner localization zones with high intensities of effective plastic strain appear at the fix end of the bar.

In Fig. 26, the propagation of the localization band in term of effective plastic strain along the wet bar has been plotted sequentially at several times. It can be observed that the width of the localization zone increases after wave reflection but the speed of expansion of the zone diminishes gradually. After a certain time, a constant localization band width $w = 13.2\,\text{mm}$ is obtained.

The developments of the compressive stresses along the saturated bar with permeability 2.0e−02 m/s has been plotted at several times in Fig. 27. It shows the significant stress reduction due to strain localization at the fixed end of the bar.

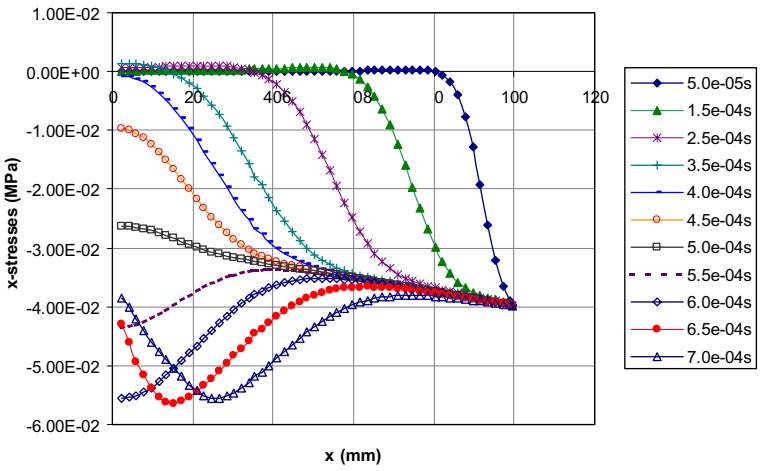

Fig. 27. In time development of x-stresses in saturated bar.

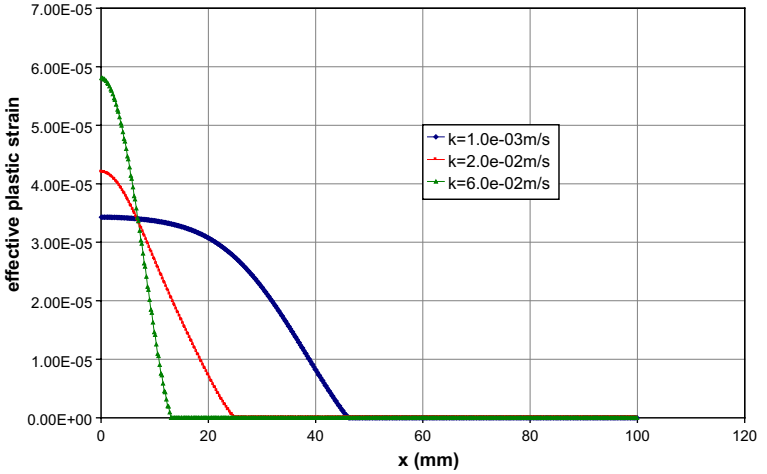

Fig. 28. Effective plastic strain distribution along wet bar with different permeabilities.

As indicated before, the internal length scale naturally included in the multiphase material model depends on several material parameters and in particular on the permeability. In order to illustrate the influence of the permeability on the width of the shear band through the internal length scale, three permeability values of 6.0e−02, 2.0e−02 and 1.0e−03 m/s are selected for comparisons. According to Zhang et al. (1999), the internal length scale for localization analysis in one-dimensional multiphase materials under dynamic loading condition can be determined by

$$l \cong \frac{2c_m\eta}{k_w \cdot K^2 \cdot \bar{\alpha}^2 \cdot S_w \cdot Q^*} \tag{1}$$

where

$$c_m = \sqrt{\frac{E_2}{\rho}}, \quad \eta = \frac{E_2}{Q^*}, \quad E_2 = \bar{\alpha}^2 S_w Q^* + \bar{H} \tag{2}$$

in which $\bar{\alpha}$ is Biot's constant, K is the wave number, k_w is soil permeability, Q^* is a parameter related to the compressibility of the solid and the water components and $\bar{H}$ is the material softening modulus. For the 'Eastern Scheldt' sand, an average softening modulus $\bar{H} = -450.0$ MPa is assumed. On the basis of Eq. (1), for permeability values of 6.0e−02, 2.0e−02 and 1.0e−03 m/s, the length scale is computed as 0.0096, 0.028 and 0.576 m, respectively, indicating the strong influence of permeability on regularization.

The numerically determined localization zones of the three cases are shown in Fig. 28. It can be observed that the width of the zone in the saturated bar increases indeed when the soil permeability is decreased highlighting thus the sensitivity of the plastic zone to the permeability values.

Example 2: Three-dimensional specimen

In the second example, the mesh sensitivity issue is demonstrated by means of a three-dimensional saturated specimen subjected to triaxial loads, see Fig. 1. This specimen has a cubic shape with impermeable boundaries. Displacement controlled loads are applied on top of the specimen throughout the analysis. The 'Eastern Scheldt' dense sand is chosen again for this numerical study. The model parameters are shown in Table 1. A permeability of $k_w = 1.0\text{e}{-06}$ m/s is specified for the analysis.

In order to verify mesh insensitivity of the model, in front view, three finite element meshes consisting of 200, 450, 800 elements respectively are examined. The three deformed meshes, at the same level of vertical

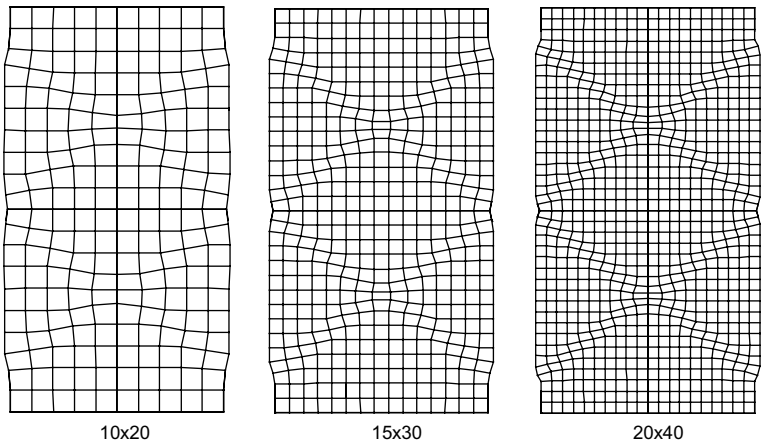

Fig. 29. Deformation patterns of the three meshes (saturated).

displacement, are compared in Fig. 29. The corresponding contours of effective plastic strain are shown in Fig. 30.

The load–displacement diagrams in Fig. 31 exhibit proper convergence to a unique solution and the same convergence is visible in the deformation patterns in Fig. 29 and contour plots of effective plastic strain in Fig. 30.

It should be noted that the influences of permeability on the development of localization in this three-dimensional specimen has been shown already in Fig. 5. It is observed that, for specimens with lower permeability, the plastic zone spreads over the whole structure, Fig. 5(c).

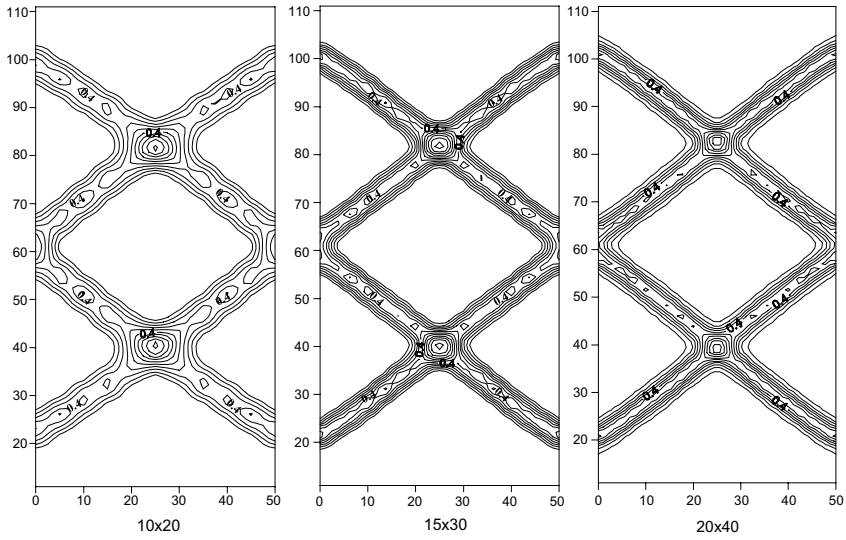

Fig. 30. Contour plots of the effective plastic strain in the three meshes (saturated).

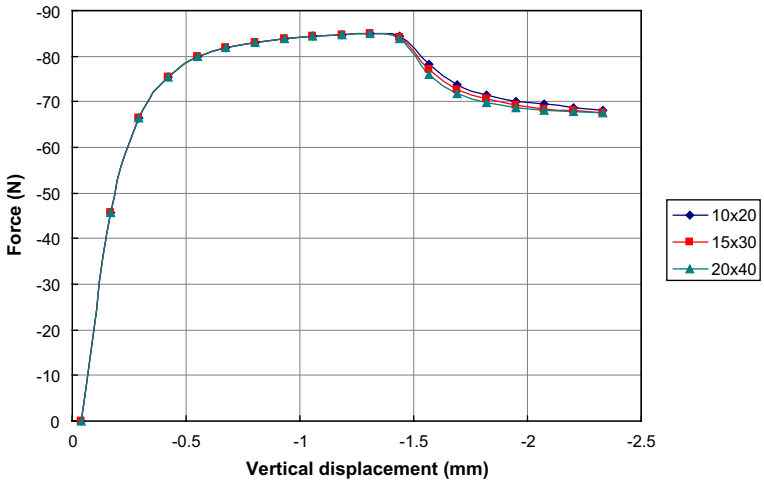

Fig. 31. Load–displacement diagrams corresponding to three meshes.

In conclusion, it can be stated that, because of the regularization provided by the fluid component, the model can provide consistent and satisfactory modeling of strain localization in porous media and avoid spurious mesh dependence. The regularization effect introduced by the gradient term of the continuity equation depends on the values of permeability. As the coupling effect between the solid and the fluid components diminishes, mesh sensitivity reemerges. This is similar to the case of a single phase solid where mesh sensitivity reappears as soon as the magnitude of the regularizing parameter of a rate or gradient sensitive material model diminishes, Loret and Prevost (1990) and Sluys (1992).

4. Conclusions

Strain localization has been observed in many geotechnical engineering problems. Gaining a better understanding of the mechanics and physics of strain localization is important for design and exploitation purposes.

Based on the numerical studies, the following conclusions can be drawn:

1. Soil permeability affects the degree of coupling between the solid and fluid phases and it plays an important role in the initiation and development of strain localization.
2. In undrained conditions, due to the incompressibility of the fluid, the tendency to dilate will build up water suction in the specimen. The induced water suction leads to soil shear strength increases. However, water suction can only delay but not preclude the development of strain localization in the specimen.
3. Another important observation is that strain localization in specimens under undrained condition always coincides with fluid cavitation. There is a physical connection between these two phenomena. It is cavitation of the pore water that leads to strain localization, and not vice versa.
4. The draining conditions can influence significantly the onset and development of strain localization. Under drained conditions, strain localization in the specimen occurs earlier than in undrained conditions. The magnitude of the maximum force at the onset of localization in an undrained specimen is higher than in a drained one. The intensity of the effective plastic strain in the shear band is significantly influenced by the draining conditions.
5. Shear band patterns depend on the thickness of the specimen. Bulging of the specimen becomes significant when the thickness is increased. As the specimen bulges, well-defined central cones develop. The cones are delineated by the shear bands. The localization zones inside the 3D specimen are not perfectly planar. Localization of large inelastic strains at the shear bands divides the specimen into well-defined blocks that, at the final stages of specimen response, move with respect to each other like rigid bodies. The transition among the shear band patterns is smooth and always associated to the specimen thickness variation.
6. The regularization effect introduced by the gradient term of the continuity equation indeed can provide consistent and satisfactory modeling of strain localization in porous media and avoid spurious mesh dependence. The internal length scale naturally included in the model depends on the values of permeability. As the coupling effect between the solid and the fluid components diminishes, mesh sensitivity reemerges.

References

Arthur, J.R.F., Dunstan, T., Al-Ani, Q.A.J.L., Assadi, A., 1977. Plastic deformation and failure in granular media. Geotechnique 27 (1), 53–74.

Desrues, J., 1996. Strain localization in geomaterials. Experimental basis. In: 8th European Autumn School, Bifurcation and Localization in Geomaterials. ALERT/Geomaterials, Grenoble. pp. 31–32.

Desrues, J., Chambon, R., Mokni, M., Mazerolle, F., 1996. Void ratio evolution inside shear bands in triaxial sand specimens studied by computed tomography. Geotechnique 46 (3), 529–546.

Desrues, J., Lanier, J., Stutz, P., 1985. Localization of the deformation in tests on sand sample. Engineering Fracture Mechanics 21 (4), 909–921.

Eringen, A.C., Edelen, D.G.B., 1972. On non-local elasticity. International Journal of Engineering Science 10, 233–248.

Gawin, D., Sanavia, L., Schrefler, B.A., 1998. Cavitation modelling in saturated geomaterials with application to dynamic strain localization. International Journal for Numerical Methods in Fluids 27, 109–125.

Han, C., Vardoulakis, I.G., 1991. Plane-strain compression experiments on water-saturated fine-grained sand. Geotechnique 41 (1), 49–78.

Harireche, O., Loret, B., 1992. 3-D dynamic strain-localisation: shear-band pattern transition in solids. European Journal of Mechanics A/Solids 11 (6), 733–751.

Karstunen, M., 1999. Numerical modelling of strain localization in dense sands. Ph.D. Thesis, Acta Polytechnica Scandinavica, Civil Engineering and Building Construction, Finland.

Lade, P.V., 1982. Localization effects in triaxial tests on sand. In: Proc. IUTAM Conf. on Deformation and Failure of Granular Media, Delft, pp. 461–471.

Liu, X., 2003. Numerical Modelling of porous media response under static and dynamic load conditions. Ph.D. Thesis, Faculty of Civil Engineering, Delft University of Technology, Netherlands.

Liu, X., Scarpas, A., Blaauwendraad, J., 2001. Finite element investigation of localization in porous media. In: Desai, C.S. et al. (Eds.), Computer Methods and Advances in Geomechanics. Balkema, Rotterdam, pp. 559–564.

Leroy, Y., Ortiz, M., 1990. Finite element analysis of transient strain localization phenomena in frictional solids. International Journal for Numerical and Analytical Methods in Geomechanics 14, 93–124.

Loret, B., Prevost, J.H., 1990. Dynamic strain localisation in elasto(visco-)plastic solids, Part 1. General formulation and one-dimensional examples. Computer Methods in Applied Mechanics and Engineering 83, 247–273.

Loret, B., Prevost, J.H., 1991. Dynamic strain localisation in fluid-saturated porous media. ASCE. Journal of Engineering Mechanics 11, 907–922.

Mokni, M., 1992. Relations entre déformations en masse et déformations localisées dans de matériaux granulaires. Thèse de doctorat Thesis. UJF-INPG, Grenoble.

Mokni, M., Desrues, J., 1998. Strain localization measurements in undrained plane-strain biaxial tests on Hostun RF sand. Mechanics of Cohesive-Frictional Materials and Structures 4, 419–441.

Mühlhaus, H.-B., Aifantis, E.C., 1991. A variational principle for gradient plasticity. International Journal of Solids and Structures 28, 845–857.

Mühlhaus, H.-B., Vardoulakis, I., 1987. The thickness of shear bands in granular materials. Geotechnique 37 (3), 271–283.

Needleman, A., 1988. Material rate dependence and mesh sensitivity in localization problems. Computer Methods in Applied Mechanics and Engineering 67, 69–85.

Rice, J.R., 1985. On the stability of dilatant hardening for saturated rock masses. Journal of Geophysical Research 80, 1531–1536.

Rudnicki, J.W., 1984. Effect of dilatant hardening on the development of concentrated shear-deformation in fissured rock masses. Journal of Geophysical Research 89 (B11), 9259–9270.

Schrefler, B.A., Majorana, C.E., Sanavia, L., 1995. Shear band localization in saturated porous media. Archives of Mechanics 47, 577–599.

Schrefler, B.A., Sanavia, L., Majorana, C.E., 1996. A multiphase medium model for localization and post-localization simulation in geomaterials. Mechanics of Cohesive-Frictional Materials and Structures 1, 95–114.

Sluys, L.J., 1992. Wave propagation, localisation and dispersion in softening solids. Ph.D. Thesis, Faculty of Civil Engineering, Delft University of Technology, Netherlands.

Sluys, L.J., de Borst, R., 1992. Wave propagation and localization on a rate-dependent cracked medium—model formulation and one-dimensional examples. International Journal of Solids and Structures 29, 2945–2958.

Tatsuoka, F., Nakamura, S., Huang, C.C., Tani, K., 1990. Strength anisotropy and shear band direction in plane strain tests of sand. Soils and Foundations 30 (1), 35–54.

Vardoulakis, I., 1979. Bifurcation analysis of the triaxial test on sand samples. Acta Mechanica 32, 35–54.

Vardoulakis, I., 1980. Shear band inclination and shear modulus of sand in biaxial tests. International Journal for Numerical and Analytical Methods in Geomechanics 4, 103–119.

Vardoulakis, I., 1986. Dynamic stability analysis of undrained simple shear on water-saturated granular soils. International Journal for Numerical and Analytical Methods in Geomechanics 10, 177–190.

Vardoulakis, I., 1996a. Deformation of water saturated sand: I. Uniform undrained deformation and shear banding. Geotechnique 46 (3), 441–456.

Vardoulakis, I., 1996b. Deformation of water saturated sand: II. Effect of pore water flow and shear banding. Geotechnique 46 (3), 457–472.

Zhang, H.W., Sanavia, L., Schrefler, B.A., 1999. An internal length scale in dynamic strain localization of multiphase porous media. Mechanics of Cohesive-Frictional Materials and Structures 4, 443–460.

Zhang, H.W., Schrefler, B.A., 2001. Uniqueness and localization analysis of elastic-plastic saturated porous media. International Journal for Numerical and Analytical Methods in Geomechanics 25, 29–48.